To be published in *Surface Scattering and Diffraction for Advanced Metrology II*,
Zu-Han Gu and Alexei A. Maradudin, Eds. Proc. SPIE **4780** (2002).

Measurement of lithographic overlay by light scattering ellipsometry

Thomas A. Germer

Optical Technology Division
National Institute of Standards and Technology
Gaithersburg, MD 20899

ABSTRACT

We demonstrate a measurement of lithographic overlay using light scattering ellipsometry. In the limit of small amplitude surface topography, the polarization of light scattered by the two interfaces of a dielectric film can be decomposed into the roughness of each interface and the complex degree of phase correlation. For two identical but offset roughness functions, the degree of phase correlation will show oscillations, whose frequency in the spatial frequency domain will be given by the overlay distance Δx. The method is tested using a shallow pseudorandom binary 1-D grating, photolithographically produced on a silicon wafer and again on a spin-on glass layer deposited onto the wafer.

Keywords: ellipsometry, films, lithography, overlay, roughness, scattering, topography

1. INTRODUCTION

A recently performed set of measurements demonstrated that light scattering ellipsometry (LSE) can be used to simultaneously determine the roughness of two interfaces of a dielectric layer on silicon.[1,2] The analysis, using first-order vector perturbation theory,[3] assumes that the field scattered by the roughness of each interface is independent of the other interface roughness and proportional to the Fourier transform of the surface height function. Using an appropriate incident polarization, one that yields a different polarization state for roughness from each interface, the resulting scattered Stokes vector intensity can be converted to the roughness of each interface and the complex degree of phase correlation between the interfaces. The method is very similar to determining film thickness using specular ellipsometry, except that, by performing the ellipsometry measurement on the diffusely scattered light, the variations in the thickness, i.e. roughness, are probed. Another study performed a similar analysis for scattering from roughness and material inhomogeneity of steel surfaces, yielding information about the phase correlation between the two scattering sources.[4]

Typically, for a naturally grown film on a substrate, the roughness of both interfaces will be expected to have a phase correlation coefficient having no imaginary component. That is, there will be no preference for the conformal roughness to be shifted in one direction or another. However, one can artificially create a roughness pattern in one interface, deposit a film that planarizes the surface, and then create the same roughness pattern offset by a small distance Δx. In this case, the correlation coefficient will be complex, given by $\exp(2\pi \mathrm{i}\, f \Delta x)$, where f is the spatial frequency determined by the scattering geometry via the Bragg relationship. This manuscript presents the first known attempt to perform this measurement.

2. THEORY

A full description of the first-order perturbation theory of scattering by the roughness of each of the two interfaces of a dielectric film can be found in Ref. 2. The theory assumes that the roughness amplitude is much smaller than the optical wavelength and that the interfaces to not interact with each other. The theory extends the work of Elson,[3] which traces its roots to the single interface work of Rice[5] and Barrick[6]. In this approximation, the Jones matrix for scattering by each interface is a function only of the optical constants of the substrate and the film, the thickness of the film, the geometry of the measurement (incident polar angle θ_i, incident azimuthal angle ϕ_i, scattering polar angle θ_r, and scattering azimuthal angle ϕ_r), the wavelength of the light, λ, and the Fourier transform of the surface roughness function. The surface roughness functions enter into the scattering matrices only as a factor, so that the polarization properties of

the scattering are not a function of the surface roughness function. We can then consider the net Jones scattering matrix to be

$$\mathbf{A}_\mathrm{T} = \mathbf{A}_\mathrm{b} Z_\mathrm{b} + \mathbf{A}_\mathrm{e} Z_\mathrm{e}\,, \tag{1}$$

where $\mathbf{A}_\mathrm{b}$ and $\mathbf{A}_\mathrm{e}$ are the scattering matrices (per unit roughness) for the buried and exposed interfaces, respectively, and Z_b and Z_e are the Fourier transforms of the surface roughness functions for the buried and exposed interfaces, respectively. The matrices $\mathbf{A}_\mathrm{b}$ and $\mathbf{A}_\mathrm{e}$ depend upon the scattering geometry, the optical properties of the substrate and the coating, the thickness of the coating, and the wavelength λ. When the surfaces are correlated and of equal amplitude, the scattering matrices from each interface add directly to yield the total scattering matrix. That is

$$\mathbf{A}_\mathrm{T}(0) = (\mathbf{A}_\mathrm{b} + \mathbf{A}_\mathrm{e}) Z_\mathrm{b}\,. \tag{2}$$

If the two surfaces are identical aside from an overlay distance Δx, then the total scattering matrix will be

$$\begin{aligned} \mathbf{A}_\mathrm{T}(\Delta x) &= \mathbf{A}_\mathrm{b} Z_\mathrm{b} + \mathbf{A}_\mathrm{e} Z_\mathrm{e} \\ &= \mathbf{A}_\mathrm{b} Z_\mathrm{b} + \mathbf{A}_\mathrm{e} Z_\mathrm{b} \exp(-2\pi \mathrm{i} f \Delta x) \\ &= [\mathbf{A}_\mathrm{b} + \mathbf{A}_\mathrm{e} \exp(-2\pi \mathrm{i} f \Delta x)] Z_\mathrm{b}, \end{aligned} \tag{3}$$

where f is the spatial frequency probed by the geometry, determined by the Bragg relationship. For the geometry used for this experiment, where $\theta_\mathrm{i} = \theta_\mathrm{r}$, the spatial frequency is given by

$$f = 2\sin(\theta_\mathrm{i})\sin[(\phi_\mathrm{r} - \phi_\mathrm{i})/2]/\lambda\,. \tag{4}$$

A non-zero overlay distance Δx is expected to cause interference fringes between the scattered light from the two surfaces. Since the scattering by the two interfaces yield different polarizations, this interference is expected to be manifested as oscillations in the polarization state. The larger the overlay distance, the finer these oscillations will be observed.

A Stokes vector intensity can be decomposed into a partially incoherent sum of any two non-degenerate Jones matrices.[2] The four Stokes vector elements map onto the scaling factors for each Jones matrix and the complex degree of phase correlation. For the case given in Eq. (1) above, the phase correlation function C is given by

$$C = \left\langle Z_\mathrm{b} Z_\mathrm{e}^{\,*} / \left(|Z_\mathrm{b}||Z_\mathrm{e}| \right) \right\rangle. \tag{5}$$

For the case of the pattern offset by Δx, the phase correlation function is given by

$$C = \exp(-2\pi \mathrm{i} f \Delta x)\,. \tag{6}$$

Ref. 2 presents an algorithm for performing the decomposition and determining the phase correlation function C. This decomposition is valid when only two scattering sources exist, the scattering mechanisms are non-depolarizing, and there are no interactions or cross-coupling between the scattering sources.

3. EXPERIMENT

3.1. Overlay structure

Figure 1 shows the layout of the mask used to produce the lithographic pattern. The mask contained eight rectangular regions, each containing four sub-regions, each in turn measuring 5 mm by 16.5 mm. In between the regions are marks for mask alignment. Half of the regions (C, D, E, and F) contain periodic gratings (1.5 μm lines with a 15 μm period) and were not used in this study. The other eight regions (A, B, G, and H) contained an identical pattern of pseudorandomly placed lines having widths 1.5 μm, 1.8 μm, 2.2 μm, and 2.6 μm, each extending the entire 5 mm width of the region. One line of each width was randomly placed within each 81 μm, with a minimum distance of 1.5 μm between lines, yielding an average line-to-space ratio of 10 %. Each sub-region thus has a total of 812 lines covering its

16.5 mm length. The pattern was written by electron beam lithography using a 0.1 μm address, and the critical dimension of 1.5 μm was maintained within 0.25 μm. The regions were situated on the mask so that if the mask is rotated 180º, the patterns lie on top of themselves, with progressive offsets ranging from –0.75 μm to 1.25 μm. (The seemingly odd pattern of offsets was due to an error in the mask design, which the author discovered after the mask was produced.)

Several steps were necessary to produce a shallow overlay structure on the wafer. Bare wafers were oxidized in dry O_2 to produce an approximately 79 nm thermal oxide. Photoresist was applied to the wafers, and they were exposed by contact to the mask oriented in the "normal" direction. After photoresist development, the wafers were etched in buffered hydrofluoric acid to remove the oxide under the pattern. The photoresist was then removed, and the wafers were further oxidized, so that the features had a total oxide thickness of approximately 68 nm, while the spaces had a total oxide thickness of approximately 110 nm. The oxide layer was then etched completely in buffered hydrofluoric acid, leaving a wafer with topographic features with depth of approximately 37 nm.

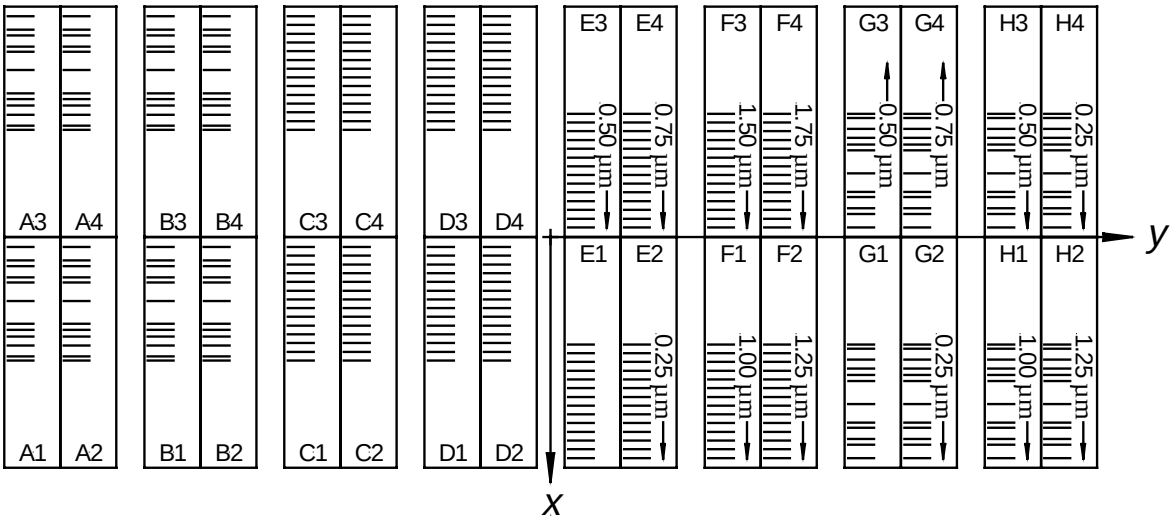

Figure 1: The layout of the mask used to produce the pattern described in this paper. The randomly spaced lines are replicated in regions A, B, G, and H in the orientations shown. Periodic gratings are found in regions C, D, E, and F. The offset magnitudes and directions are shown for all sub-regions having non-zero offset. The mask is designed to be rotated onto itself to generate a range of overlay distances.

The wafers were then spin-coated with a flowable oxide (FoX-14 from Dow Corning[7]), and given the recommended treatment to planarize the exposed interface and convert it to oxide. Planarization was incomplete, but sufficient to observe the pattern and the alignment marks in a mask aligner. The final thickness of the oxide was approximately 250 nm, and its index of refraction was measured to be approximately 1.443. Photoresist was then applied to the wafers, and the wafers were exposed to the mask rotated 180º from the "normal" orientation. Alignment of the mask, which was complicated by the shallowness of the previously produced features, was performed with an accuracy of better than 10 μm at the center of the wafer. After photoresist development, the wafers were etched in hydrofluoric acid to produce features with a depth of approximately 28 nm.

Atomic force microscope (AFM) images were obtained for eight different overlay sub-regions where light scattering measurements were performed. Figures 2 and 3 show results from the overlay of sub-region H3 onto sub-region A2 (designated H3/A2). Two patterns can be observed: one which is shallower and has more sloping walls, and the other which is deeper and has steeper walls. The shallower features result from incomplete planarization of the surface, which allows the buried interface features to replicate partially on the exposed interface. The pattern shown in Figs. 1 and 2 has an offset distance of approximately 6.2 μm. Figure 3 includes an approximate assignment of the two patterns to help guide the reader.

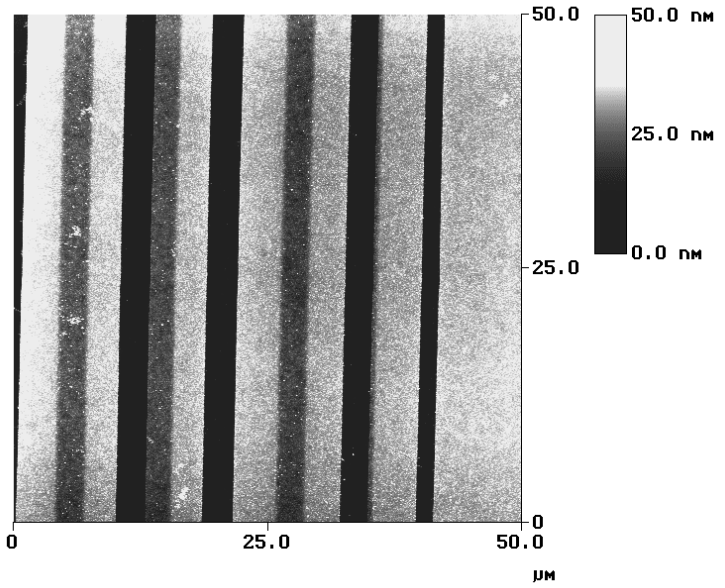

Figure 2. Atomic force microscope image of the exposed interface of part of the test structure in sub-region H3/A2. The shallower features result from feedthrough of features on the lower interface and are offset by approximately 6.2 μm from the deeper features, which exist only on the exposed interface.

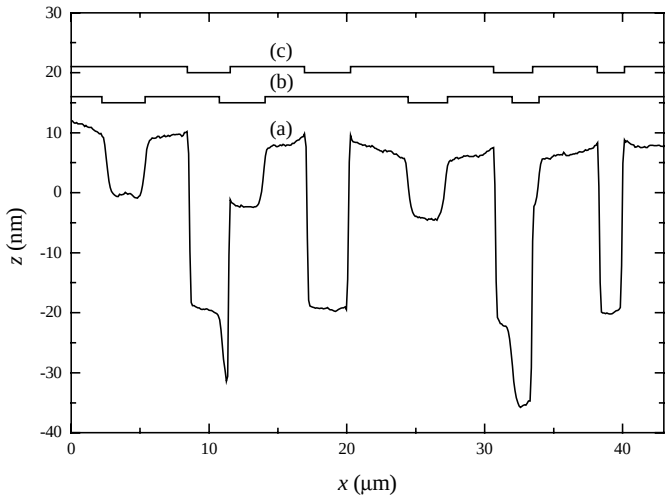

Figure 3. An average line scan (a) across the AFM image shown in Fig. 2. The shallow features are approximately 10 nm deep and have smoothly sloping walls. The deeper features are approximately 28 nm deep and have very steep walls. The two overlaid patterns, (b) and (c), are shown above the line scan.

3.2. Optical Scattering Measurements

The Goniometric Optical Scatter Instrument (GOSI), described in detail elsewhere,[8,9] was used to perform the measurements, using λ = 532 nm. The instrument measures the Stokes vector intensity of scattered light as a function of incident direction (parameterized by polar angle θ_i and azimuthal angle ϕ_i), scattering direction (parameterized by polar angle θ_r and azimuthal angle ϕ_r), and incident polarization state (linear polarization parameterized by angle η_i, measured with respect to s-polarization). Since the validity of the first-order theory is improved for large polar incident

and scattering angles, the measurements were carried out with $\theta_i = -\theta_r = -60°$. Since the structures were one-dimensional, the azimuthal angles were varied such that $\phi_i = 90° - \alpha$ and $\phi_r = 90° + \alpha$, where the plane defining $\phi_i = 0°$ and $\phi_r = 0°$ corresponds to that defined by the surface normal and the grating direction. In order to achieve high polarimetric contrast between the two interfaces, the incident polarization was varied according to $\eta_i = 45° - \alpha$. The parameter α was varied from 0° to 85°, so that $\phi_r - \phi_i$ varied from 0° to 170°. In each direction, the Stokes vector intensity of the scattered light was measured. The measurements were carried out for eight of the overlaid sub-regions at one end of the layout. An entire scan at a single location takes approximately 2.5 h. However, the instrument is not optimized for speed, and the results presented here could be acquired in a substantially shorter period of time with optimized instrumentation.

4. RESULTS AND DISCUSSION

Figure 4 shows the degree of circular polarization, P_C, measured as a function of the spatial frequency f. As predicted by the expected interference between the scattering by the buried and exposed interface roughnesses, oscillations in the polarization state can be observed. The depth of the oscillations is large, with the light varying between nearly orthogonal polarization states. The period of these polarization oscillations is relatively uniform over the scattering range, although the amplitude dampens somewhat. While one can measure the frequency of the oscillations of P_C to obtain an overlay distance, changes of the polarization state that are expected to occur even for a perfect overlay, which result due to the differences in scattering geometry would not be properly taken into account.

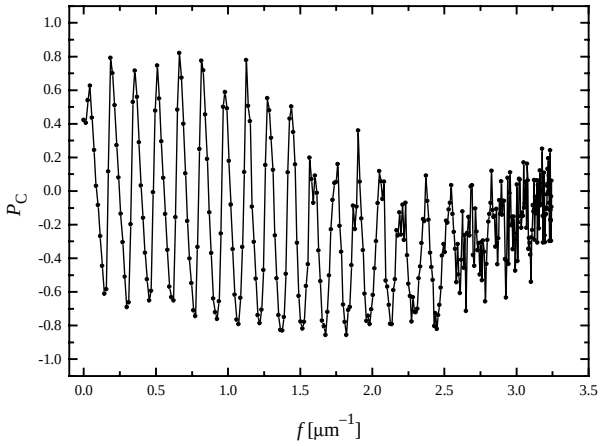

Figure 4. The degree of circular polarization as a function of the spatial frequency measured in the sub-region H3/A2. The scattering measurement was carried out at the same location as the AFM image and line scan shown in Figs. 2 and 3.

The full Stokes vectors for all of the data were decomposed into roughness parameters. Figure 5 shows the phase correlation function C resulting from the decomposition of the Stokes vector for the same sub-region shown in Figs. 2–4. The real and imaginary parts of C are approximately 90° out of phase with one another and are sinusoidal, so that the function C traces out circles in the complex plane. This behavior is exactly that predicted by Eq. (6). The frequency of oscillations, which can be interpreted as the overlay distance, is approximately 6.39 μm for the data shown in Fig. 5. At high spatial frequency, the amplitude of the oscillations decay and become noisy, which is a result of non-idealities in the lithography and the mask, poorer polarimetric discrimination at these spatial frequencies, residual interactions between the two interfaces, and the imperfect treatment of the feedthrough of the buried interface pattern onto the exposed interface.

While we are not carrying out a full analysis of the uncertainties in the measurement, a couple of tests allow us to assess the possible accuracy of the method. In the first, we compare the overlay distance measurements obtained by light scattering ellipsometry with those obtained using AFM. Figure 6 shows results from the eight different measurements. The results show data scattered about the straight line defined as perfect agreement. The difference between the

overlay distances measured by AFM and by light scattering ellipsometry has an average of 0.09 μm, while the standard deviation is 0.22 μm, suggesting that there are no large systematic errors. We must note that there are uncertainties associated with the AFM data as well as the light scattering ellipsometry data, which are unknown at this time.

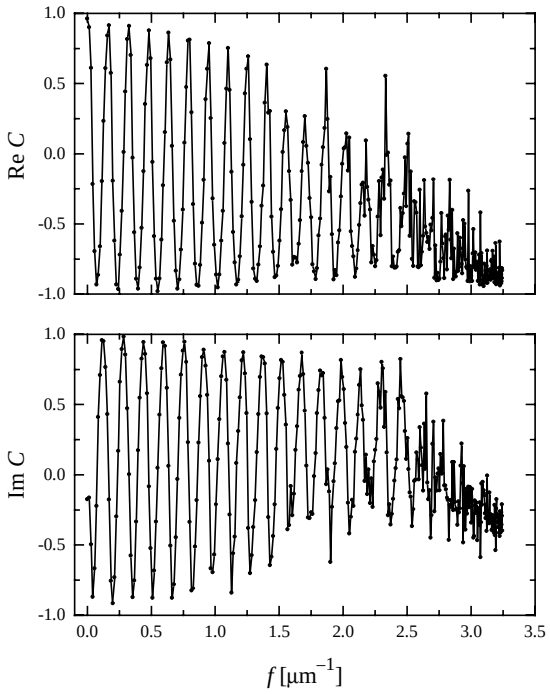

Figure 5. The real and imaginary parts of the phase correlation coefficient *C* extracted from the measurement of the scattered Stokes vector, of which the degree of circular polarization is shown in Fig. 4. The period of the oscillations of *C* is approximately 0.156 μm^{-1}, corresponding to an overlay distance of approximately 6.39 μm.

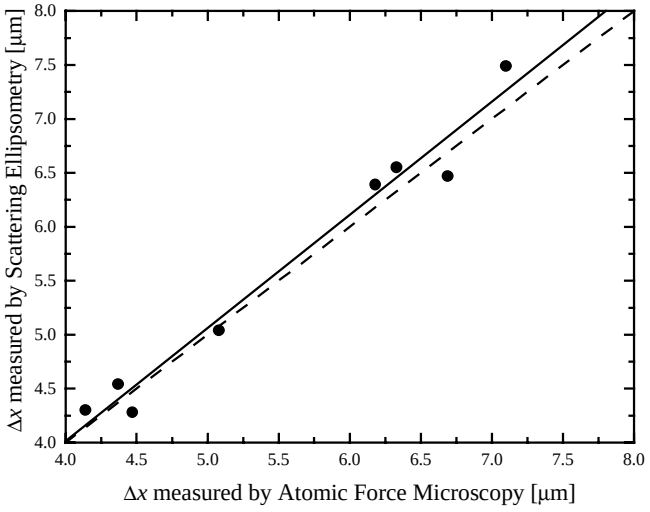

Figure 6. The overlay distance, Δ*x*, extracted from the light scattering ellipsometry measurements versus that measured by atomic force microscopy. The solid line is a best fit to the data, while the dashed line represents an ideal correlation.

Another test is to check for consistency of the overlay measurements with the notion that the overlay may have a fixed rotation in addition to a translation. Figure 7 shows the overlay distance measured by light scattering ellipsometry, corrected for the intentional overlay distances shown in Fig. 1, as a function of horizontal position along the wafer. The non-zero slope of these points is believed to be mostly a result from an overlay rotation. Linear-least-square fits to the points yield slopes of (0.13±0.01) μm/mm and (0.10±0.01) μm/mm, which corresponds to rotation angles of 0.0075° and 0.0057°, respectively. That these rotation angles are not the same may be due to inaccuracies in the manufacture of the mask. The root-mean-square of the deviation of the points from the lines is 0.06 μm. Since we have not carried out a full analysis of the uncertainties in the measurements, we do not know if the observed deviations represent the uncertainties inherent in the method. That is, a portion of them may result from uncertainties in the method, while there may also be distortions on the original mask.

The use of a random grating, rather than a periodic one, was chosen since it allows a continuous measurement of scatter with angle, enabling the periodicity of the polarization state to be measured and allowing potentially arbitrary overlay distances. For a periodic surface, the scattering is limited to discrete points, making this analysis more difficult. In particular, the results are rather insensitive to errors in our knowledge of the full profile of both interfaces and of the film thickness. This can be seen by the fact that the period in the oscillations observed in the directly measured P_C match those observed in the model-extracted value C.

Light scattering ellipsometry can also be applied to two-dimensional patterns, enabling two-dimensional overlay vectors to be determined. However, the decomposition of the Stokes vector into the roughness statistics requires that only the roughnesses of the two interfaces contribute to the scattering. Two-dimensional random features diffusely scatter light in all directions, instead of in a plane as is done by one-dimensional features. Any other sources of scatter, such as particles, film defects, or film inhomogeneities can make the decomposition invalid. Nevertheless, the observation that the overlay distance can be extracted simply from the period of oscillations of the polarization state suggests that the same analysis may hold, provided all of the sources of scatter yield slowly varying contributions to the polarization.

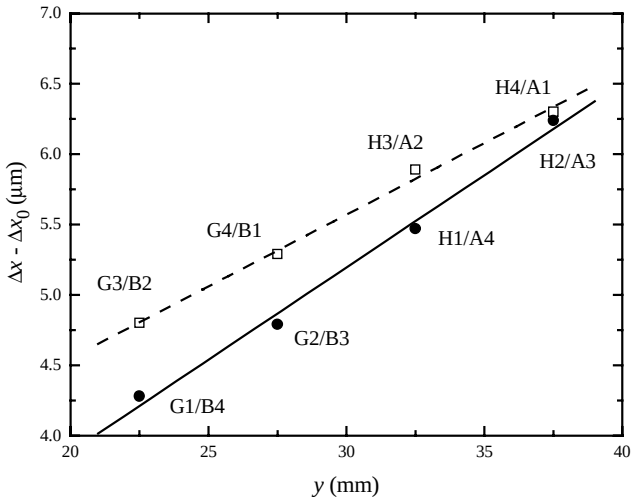

Figure 7. The overlay distance Δx measured by light scattering ellipsometry corrected for the intentional overlay distance Δx_0. The solid symbols correspond to one row along the wafer, while the open symbols correspond to another row. The pattern sub-regions corresponding to the exposed and buried interface are shown for each point. The dashed and solid lines represent linear-least-square fits to the respective data points. The abscissa is the distance from the center of the wafer.

The topography used in this study was chosen to be as shallow as possible in order to allow for use of first-order vector perturbation theory in the analysis, and deep enough to enable the observation of the features in the mask aligner. (Further steps could have been taken to enable alignment of both patterns to a much more visible, pre-etched,

alignment pattern.) The analysis, however, relies upon the thin film thickness being uniform, so it is best applied when the two interfaces are correlated and of similar roughness. To observe clear interference oscillations, however, the overlay distance must be considerable. For large overlay distances, the average film thickness is relatively constant, albeit there are many random variations. These variations would be expected to yield increased depolarization. The polarization oscillations should still exist with the appropriate period.

Ultimately, the method must be extended to deeper topographic features in order for the method to be applied in production line environments. In this case, the use of first-order theories would be inappropriate. However, it may be possible to create structures that show each of the two surfaces, without the other, allowing the scatter from each of the two scattering sources to be isolated. Furthermore, as long as the scatter from each feature is slowly varying in angle compared to the expected period of oscillations, that period can be obtained. However, the center of the scattering may not correspond to the center of the features, if the features are not symmetric. Further work is needed to establish the use of the method for larger topographies.

5. SUMMARY

We present a new method, based upon light scattering ellipsometry, for measuring lithographic overlay. The method uses a test structure with a shallow one-dimensionally random pattern. Polarization oscillations resulting from the interference between scattering by topography of one interface with that by topography of the other interface are predicted, observed, and their periods correlate well with AFM measurements.

ACKNOWLEDGEMENTS

The author would like to thank Dr. Michael Fasolka for assisting in the atomic force microscopy images and Mr. Russell Hajdaj for assisting in the fabrication of the samples.

REFERENCES AND NOTES

1. T. A. Germer, "Measurement of roughness of two interfaces of a dielectric film by scattering ellipsometry," Phys. Rev. Lett. **85,** 349-352 (2000).

2. T. A. Germer, "Polarized light scattering by microroughness and small defects in dielectric layers," J. Opt. Soc. Am. A **18,** 1279-1288 (2001).

3. J. M. Elson, "Multilayer-coated optics: guided-wave coupling and scattering by means of interface random roughness," J. Opt. Soc. Am. A **12,** 729-742 (1995).

4. T. A. Germer, T. Rinder, and H. Rothe, "Polarized light scattering measurements of polished and etched steel surfaces," in *Scattering and Surface Roughness III*, Z.-H. Gu and A. Maradudin, Eds., Proc. SPIE **4100**, 148-155 (2000).

5. S. O. Rice, "Reflection of Electromagnetic Waves from Slightly Rough Surfaces," Comm. Pure and Appl. Math. **4,** 351-378 (1951).

6. D. E. Barrick, "Rough Surfaces," in *Radar Cross Section Handbook*, George T. Ruck Ed. (Plenum, New York, 1970) Chap. 9.

7. Certain commercial equipment, instruments, or materials are identified in this paper in order to specify the experimental procedure adequately. Such identification is not intended to imply recommendation or endorsement by the National Institute of Standards and Technology, nor is it intended to imply that the materials or equipment identified are necessarily the best available for the purpose.

8. T. A. Germer and C. C. Asmail, "A goniometric optical scatter instrument for bidirectional reflectance distribution function measurements with out -of-plane and polarimetry capabilities," in *Scattering and Surface Roughness*, Z.-H. Gu and A. A. Maradudin, Eds., Proc. SPIE **3141**, 220-231 (1997).

9. T. A. Germer and C. C. Asmail, "Goniometric optical scatter instrument for out-of-plane ellipsometry measurements," Rev. Sci. Instr. **70,** 3688-3695 (1999).